Int. J. Appl. Math. Comput. Sci., 2026, Vol. 36, No. 2, 297–313
DOI: 10.61822/amcs-2026-0020

DESIGN OF A SMART ALARMING SYSTEM USING TRANSFER ENTROPY–BASED CAUSALITY GRAPHS

HUBERT PISIECKI [a], PAWEŁ D. DOMAŃSKI [a,*]

[a]Institute of Control and Computational Engineering
Warsaw University of Technology
Nowowiejska 15/19, 04-429 Warsaw, Poland
e-mail: {hubert.pisiecki.stud,pawel.domanski}@pw.edu.pl

This paper addresses the critical challenge of alarm floods in industrial automation systems, where cascading alarms obscure root causes of disturbances. The primary aim is to develop and validate an original smart alarming algorithm that identifies disturbance source by analyzing directional information flow between the system's process variables. The proposed methodology integrates transfer entropy (TE), an information-theoretic measure of causal relationships, with median ensemble empirical mode decomposition (MEEMD) for signal preprocessing. The scope encompasses data normalization, delay estimation via cross-correlation (CC) and mutual information (MI), causality computation using TE, and causal graph construction to visualize disturbance propagation pathways. The algorithm is validated on two systems: a Simulink multi-loop control model and the Tennessee Eastman Process (TEP)—an industrial benchmark. The proposed methodology successfully traces disturbances and validates the method's ability to identify the root cause. Key innovations include noise-resilient decomposition and dual-method delay estimation, which enhance robustness in high-dimensional systems. The method reduces alarm floods by isolating primary disturbances, even under nonlinear and noisy conditions.

Keywords: smart alarming, transfer entropy, causality analysis, MEEMD, alarm flooding, Tennessee Eastman Process.

1. Introduction

Modern industrial facilities are characterized by a high degree of automation with an extensive instrumentation and control infrastructure. While alarm systems remain essential for early fault detection, traditional methodologies based on simplistic signal thresholding fail to effectively indicate their real root cause. In practice, operators receive notifications about threshold violations, yet they cannot discern which alerts stem from the primary disturbance (see Seyed Alinezhad *et al.*, 2022). Furthermore, disturbances affecting a given process installation can propagate across interconnected systems, impacting all process variables along the causal pathway. Alarms associated with these variables are triggered *en masse*, overwhelming control operators, who cannot feasibly investigate each notification. Research names this phenomenon an alarm flood and shows that it creates a critical bottleneck (Rodrigo *et al.*, 2016).

The concept of intelligent alarming, or "smart alarming", is proposed. It leverages directional information flow analysis between process variables to isolate the root disturbance-initiating variable regardless of system complexity or nonlinear process relationships. Transfer entropy (TE) has been introduced as an information-theoretic measure of asymmetric information transfer (Schreiber, 2000). This work adopts TE because it quantifies nonlinear, directional dependencies between time series, enabling the detection of causal pathways even in noisy, high-dimensional systems. TE's application in industrial process monitoring remains relatively unexplored, particularly in scenarios involving alarm floods or cascading failures. This gap offers an opportunity for novel contributions.

Root cause analysis (RCA) in the process industry encompasses both knowledge-driven and fully data-driven methods. Causality methods allow constructing causal graphs. Their effectiveness decreases for nonlinear relationships and significant noises (Shojaie and Fox, 2022). In contrast, pattern recognition-based alarm sequence classification algorithms and deep

*Corresponding author

learning techniques might reduce alarm flood phenomena (Vogel-Heuser *et al*., 2015). However, these methods often fail to identify the root disturbance source, which makes difficult to react quickly and precisely.

TE might be useful as it quantifies asynchronous and nonlinear information flow between two temporal processes, detecting both the direction and magnitude of causal dependencies. It enables the construction of directed information flow graphs, where edges represent probable disturbance propagation pathways, offering a systematic framework.

Recent studies (Zhang *et al*., 2022; Falkowski and Domański, 2023) demonstrate TE's high performance in simulated industrial processes for detecting causal pathways and root causes of disturbances. It outperforms Granger causality (GC) in scenarios involving nonlinear dynamics and closed-loop control systems. For instance, TE's robustness in a two-tank benchmark model shows its ability to handle delayed interactions through information granulation (Zhang *et al*., 2022). Similarly, its resilience to controller-induced noise in feedback loops is addressed by Lindner *et al*. (2017b), contrasting with GC's sensitivity to such perturbations.

Transfer entropy finds applications not only in process engineering but also across numerous disciplines, underscoring its universality and efficiency in causal relationship analysis. It is used to detect directional temporal dependencies between the activity of distinct brain regions (Vicente *et al*., 2011), enabling the study of information flow within neural networks and the identification of functional connectivity between cerebral structures. Some research (Kwon and Yang, 2008) identifies directional influences between markets or financial instruments, while other works (Tongal and Sivakumar, 2021) use it to detect directional information flows between climatic variables, such as ocean surface temperature and precipitation patterns, aiding in weather analysis and forecasting.

To enhance the sensitivity and reliability of TE analysis, proper preprocessing of process signals is required. Median ensemble empirical mode decomposition proposed by Lang *et al*. (2020) is employed to extract complex temporal features from process signals, as it inherently contains both actionable information and noise components critical for disturbance analysis. Unlike classical EMD (empirical mode decomposition) (Huang *et al*., 1998), which primarily focuses on artifact filtration, MEEMD ensures the preservation and isolation of all intrinsic mode functions (IMFs), including those intrinsically linked to noise variance. The resulting signal IMF pathways constitute a robust feature set for TE analysis, where each IMF provides distinct insights into system dynamics and directional disturbance propagation among process variables.

Causality analysis is a broad concept, which can be adopted in various scenarios. Detection of the root cause is the most natural one. Control engineering started to incorporate these ideas to control performance tasks (Lindner *et al*., 2017a). However, apart from the control performance assessment context (Domański, 2020; 2025), other areas could be also targeted. Especially the research on fault detection would benefit considerably (Kościelny *et al*., 2022). The most promising property of the transfer entropy approach is its model-free calculation algorithm. We do need to identify the process model, and we escape from the dilemma (Kóscielny and Bartyś, 2025) whether the fault really exists or the model is wrong.

We must be aware that this research only aims at the detection of the reason—its place. A causality graph does not say what is wrong and what should be done (Chu *et al*., 2023; Maican *et al*., 2025). It does not address the diagnosis or recovery. Other research highlights the issues associated with the large-scale plantwide control frequent in chemical engineering (Ruiz *et al*., 2001). As the cause is not a goal, the cyber-security aspect is not explicitly addressed, though such a direction seems to be promising (Jungwirth and Hahs, 2019; Jadidi *et al*., 2022).

The primary contribution is the development and empirical validation of an advanced algorithm that unambiguously identifies the primary disturbance source in industrial systems. The basis of this approach lies in the application of TE. This ensures that the algorithm can distinguish information transfer triggering system failures from spurious signal correlations.

Another contribution is an original signal preprocessing algorithm that uses MEEMD to extract both stable and noise-related components from raw data. The synergy of these two methods allows obtaining an intelligent "smart alarming" system, which not only reduces the incidence of false alarms but, more critically, empowers operators to rapidly and precisely pinpoint the variable initiating a chain of events.

The final outcome is a prototype system, whose performance is evaluated using benchmark datasets. The metric used assesses the accuracy of identifying the source of the failure, ensuring comprehensive validation of the system's operational readiness. The approach considered allows to detecting and labeling the real cause—nothing more. Any other actions, like process or control system re-configuration, overlapping and rescue actions are not considered in this research. The algorithm should not exchange existing systems, but support them.

Finally, we assume that the DCS (distributed control system) should be the only source of information for operators and plant engineers. Thus, it is not intended to design any specific information system. Information should be suitable and clearly embedded into the DCS and its logic.

Section 2 describes the research rationale and

algorithms. Presentation of methods is concluded with an original formulation of the method procedure introduced in Section 4. Section 5 discusses experimental results, while Section 6 concludes the analysis and presents issues open for further research.

2. Alarms in industrial control systems

In industrial environments, an alarm flood refers to a sudden and overwhelming influx of alarms triggered by operational anomalies, like equipment failures, process deviations, safety hazards, or malfunction risks. This phenomenon is typically characterized by complex alarm patterns stemming from interdependent processes or devices, often obscuring the root cause and impeding timely intervention (Parvez *et al.*, 2025). It can precipitate severe operational, financial, and safety-related repercussions, particularly in complex systems.

According to the ANSI/ISA-18.2 standard *Management of Alarm Systems for the Process Industries* (ANSI/ISA, 2016), an alarm flood is defined as a situation where the alarm activation rate exceeds 10 new notifications per operator within 10 minutes. The standard recommends maintaining an average alarm frequency of no more than one alarm per 10 minutes per operator, ensuring sufficient time for event assessment and response.

While ANSI/ISA-18.2 provides guidelines for maintaining alarm system performance within acceptable thresholds, it does not define mechanisms for automated root cause identification during cascading alarm scenarios. Consequently, even when compliance with the standard's quantity and quality requirements is achieved, operators lack tools to rapidly isolate the variable initiating the alarm cascade. This gap underscores the critical need for advancing smart alarming methodologies.

Historical cases demonstrate that, irrespective of the presence or absence of formal guidelines, an alarm flood can paralyze diagnostic processes. During the restart of the isomerization unit at the BP Texas City refinery in March 2005 (Labib, 2014), operators were inundated by a deluge of alarms (exceeding several hundred per minute) triggered by cascading deviations in the distillation train, ultimately contributing to one of the deadliest refinery explosions in US history. The Three Mile Island nuclear power plant accident on March 28, 1979 (Skillman and Rempe, 2021), stands as one of the most pivotal cases illustrating the catastrophic consequences of an alarm flood. As a consequence, the reactor core partially melted, releasing radioactive gases. The Texaco Milford Haven refinery disaster on July 24, 1994 (HSE, 1997) serves as a case study of how an alarm flood obstructs root cause identification during critical failures. Crucial signals indicating mechanical failure were drowned out by repetitive, non-priority alarms. This culminated in the ignition of a gas cloud, claiming five lives and destroying 20% of the refinery's infrastructure.

The above cases illustrate that alarm floods, whether in full-scale industrial units or high-fidelity simulators, consistently mask the initiating fault. This motivates the need for "smart alarming" that analyzes directional, causality-driven relations among process variables.

2.1. Traditional alarming systems.

Traditional alarming systems are frameworks designed to monitor industrial processes and notify operators of anomalies relative to defined thresholds. According to the ANSI/ISA-18.2 standard, an alarm is defined as "an audible and/or visible means of indicating to the operator an equipment malfunction, process deviation, or abnormal condition requiring a response" (ANSI/ISA, 2016). These systems rely on static, rule-based logic, where alarms trigger when process variables exceed fixed upper or lower limits.

From the perspective of the research considered, it is crucial to properly distinguish between what is normal/abnormal and not faulty/faulty. We assume that the difference between normal and abnormal is, for instance, regular installation operation versus its startup or shutdown. In such cases causality structure differences surely exist, as we use bypasses, different control loops, safety connections, etc.

Fault is a different issue. Valve may stick during regular operation and during the startup. From the perspective of the faulty valve, both regular and startup operations are normal. Causality does not change. If we do not change information and media flows, the causality should not change. Such situations are addressed in this research.

A key limitation of traditional systems is their inability to prioritize alerts during cascading failures. When a disturbance propagates through subsystems, multiple variables may exceed their thresholds simultaneously, generating redundant or secondary alarms. Operators, faced with overwhelming notifications, struggle to distinguish the root cause from derivative alerts, delaying critical interventions. This inflexibility often results in alarm fatigue, as constant false or non-urgent alarms lead to reduced operator focus.

Traditional systems employ basic logic if-then rules and lack mechanisms to analyze causal relationships or interpret alarms. While ANSI/ISA-18.2 highlights alarm life-cycle management, it does not address root cause analysis. Without advanced analytics, these systems remain unable to handle nonlinear interactions, delayed effects, or controller-induced noise.

2.2. Smart alarming systems.

Smart alarming systems are advanced frameworks designed to enhance

industrial diagnostics by prioritizing alarms based on causal relationships and operational context. They employ dynamic, data-driven analytics to distinguish primary disturbances from secondary effects during cascading failures. By analyzing patterns, temporal dependencies, and multivariate interactions, these systems reduce alarm floods and enable operators to focus on root causes rather than symptom management. This aligns with industrial standards like ANSI/ISA-18.2, which underline actionable alerts but lack tools for automated causal inference.

Existing alarming systems mostly rely on techniques like machine learning, statistical tools, and real-time signal processing. These methods help to understand process dynamics and anticipate how disturbances will spread. Advanced algorithms identify directional dependencies between variables, filtering out redundant alerts triggered by shared noise or indirect correlations. For instance, they may infer causal pathways by analyzing time-delayed interactions or nonlinear relationships, enabling precise identification of initiating events.

Validation in industrial and simulated environments highlights alarming systems' potential to improve operational robustness. Studies demonstrate reduced alarm rates, faster root cause diagnosis, and enhanced operator decision-making during critical scenarios. By aligning alarms with broader system dynamics, smart frameworks connect theoretical process understanding with real-time diagnostics.

The proposed methodology uses various methods described below, including CC as well as information-theoretic measures such as mutual information and transfer entropy. Nonlinear signal decomposition uses a median variant of EMD to separate complex signal dynamics. The components obtained this way are subject to statistical analysis, so probability density estimation is used to measure uncertainties in causal relationships. Nonparametric methods like kernel density estimation (KDE) are utilized to capture the probabilistic nature of information transfer in industrial data.

2.3. Cross-correlation. Cross-correlation analysis evaluates the relationship between two time series, $X(t)$ and $Y(t)$, by introducing a temporal lag k between them and computing their correlation coefficient at each lag. The method involves the following steps:

1. *Lag adjustment.* For a given lag k, the time series $Y(t)$ is shifted relative to $X(t)$. For example, if $k = 2$, $Y(t)$ is aligned with $X(t-2)$.

2. *Correlation calculation.* The correlation ρ is calculated as

$$\rho_k = \frac{1}{N-k} \sum_{i=1}^{N-k} \frac{(x_i - \mu_x)(y_{i+k} - \mu_y)}{\sigma_x \sigma_y}, \quad (1)$$

where N denotes number of samples, μ mean values, and σ standard deviations.

3. *Iteration across lags.* This calculation is repeated for a range of lags (e.g., $k = -L, \ldots, k = +L$). The lag yielding the maximum absolute correlation ($\rho_{\max}$) is assumed to represent the true time delay between X and Y.

The method faces several limitations, e.g., its reliance on linear assumptions. Interactions such as valve stiction-induced oscillations or quadratic dependencies between variables may remain undetected, leading to incomplete or misleading conclusions (Bauer and Thornhill, 2008). They also show that the method assumes stationarity. Nonstationary trends, such as gradual sensor drift or operational shifts, can artificially boost correlation values, masking true transient relationships. Periodic signals produce multiple peaks of equal magnitude in the cross-correlation function due to phase wrapping. Without additional dynamic features, determining the correct delay becomes unclear. Finally, it considers data points as independent samples of a static process, ignoring changes over time. This simplification overlooks time-varying dynamics, which are critical for understanding causality in real-world systems (Yang *et al*., 2014).

Despite these limitations, CC remains a valuable tool for preliminary delay estimation in linear, stationary systems. Its usefulness increases when combined with domain knowledge or advanced nonlinear methods.

2.4. Mutual information. Mutual information (MI) (Shannon, 1948) is a statistical measure based on information theory, and serves as a generalization of the correlation coefficient. Unlike CC, MI does not assume a linear relationship between variables, making it a reliable tool for analyzing complicated dependencies (Battiti, 1994). It is defined as a reduction in uncertainty about one variable due to knowledge of another variable. Formally, MI between variables x and y is expressed as

$$I(x,y) = \sum_x \sum_y p(x,y) log_2 \left(\frac{p(x,y)}{p(x), p(y)} \right), \quad (2)$$

where $p(x)$, $p(y)$ are marginal distributions and $p(x,y)$ is the joint distribution. The value of MI is high when the variables are strongly dependent and low when they are independent.

Estimating probability distributions is essential for MI calculation. When data is limited, traditional

histograms may not perform well, leading to the use of kernel density estimation (KDE) (Beardah and Baxter, 1996). KDE ensures reliable MI values even with limited samples. It is widely used in many domains, like machine learning (Zhong and Li, 2025), bioinformatics (Rahmanian and Mansoori, 2022), neuroscience (Li *et al*., 2024), signal processing (Ge and Lin, 2023), or astronomy (Chakraborty and van Leeuwen, 2022). Its ability to capture both linear and nonlinear dependencies makes it useful in engineering tasks. MI can reveal hidden relationships that remain undetected by traditional methods.

2.5. Transfer entropy. TE is an information-theoretic measure designed to quantify directional information flow between two dynamical systems (Schreiber, 2000). Unlike MI, it directly accounts for temporal dynamics and excludes false correlations arising from shared history or common external influences. This makes it particularly suited for detecting causal interactions in highly interconnected systems, such as industrial processes.

TE measures the reduction in uncertainty about the future state of a system Y (Y_{n+1}) when including the past states of another system X ($X_n^{(l)}$), beyond what is already known from the history of Y ($Y_n^{(k)}$). Formally, TE from X to Y is defined as

$$T_{X\to Y} = \sum p\left(y_{n+1}, y_n^{(k)}, x_n^{(l)}\right) \log \frac{p(y_{n+1} \mid y_n^{(k)}, x_n^{(l)})}{p(y_{n+1} \mid y_n^{(k)})}, \tag{3}$$

where $p(\cdot)$ denotes conditional probability, k and l the embedding dimensions (typically, $l = k$). TE measures the Kullback–Leibler difference between distributions, ensuring asymmetry ($T_{X\to Y} \neq T_{Y\to X}$) and directionality.

Effective application of TE-based systems depends on several critical steps (Schreiber, 2000). First, stationarity of the time series must be verified or enforced through preprocessing, such as differencing or detrending, as nonstationary data can lead to erroneous estimates. Next, the selection of embedding dimensions (k and l) is essential; these parameters define the depth of historical states used to model dependencies. Methods like the Akaike information criterion (AIC) or false nearest neighbors analysis are commonly employed to balance model complexity and predictive power. For computational efficiency, $l = 1$ is often preferred unless system dynamics demand longer memory. Probability estimation requires careful handling to avoid wrong estimation. Techniques such as KDE or histogram binning are used to approximate conditional probabilities $p\left(y_{n+1}, y_n^{(k)}, x_n^{(l)}\right)$, though these approaches become computationally intensive for high-dimensional datasets.

Evaluated transfer entropy values allow constructing the TE-based causality graph. It is obtained according to the following procedure:

1. We calculate transfer entropy matrix $T_{X_i\to X_j} \in \mathcal{R}^{N\times N}$ evaluating its value between all variables $X_i, i = 1, \ldots, N$ in both directions, i.e., $T_{X_i\to X_j}$ and $T_{X_j\to X_i}$.
2. For each variable X_i, we find a connection with the largest transfer entropy value and select it as causality connection; each variable influences only one another variable.

Therefore, the causality graph includes only the most influential connections.

Complex industrial processes incorporate several control loops. Generally, they do not affect calculations, and even make them easier. In the case of control error signals, we already get detrended with a zero mean value time series, at least in the majority of cases. That makes TE calculations easier (Falkowski, 2022; Falkowski *et al*., 2022). We are only interested in connections between loops and do not go deeper into the internal loop structure.

An unclear situation appears once we have media flow loops, re-circulation, etc. Such occurrences are frequent in the process industry. This makes it difficult to distinguish between the root and the cause. The only help that may come is proper delay estimation. The root and the cause do not appear simultaneously. We have delays, as media flow with certain speed over a certain distance. If we are able to properly identify these delays (Knockaert and Dhaene, 2008; Hamdi *et al*., 2021), we may obtain causality estimations.

The case when a variable, or a group of variables, is isolated from the rest of the process, physically or logically, may always occur. It happens while their relationship with other elements of the installation is significantly smaller and negligible compared to an isolated (islanded) group (or groups) of variables.

Such an effect may be caused by the process structure itself, or by the basic assumption of the method saying that only the strongest relationship is taken into account. This fact refers to the main shortcut of the method—the use of only the dominant relationship. It would certainly be important to propose a more developed approach that would take into account more causal relationships, also strong but not dominant. However, this is not easy, as in the simplest approach it would use "smart" or adaptive thresholding. However, this problem itself is rather open-ended without sufficiently effective and universally applicable approaches.

The above observation implies that the obtained method results should be ideally verified by a human expert at the end of the design process.

The transfer entropy method is not universal and it has weak elements, including the following:

- there is the need to use information about a delay (this aspect is addressed in the paper);
- the method was initially designed for stationary Gaussian noises, thus it may be misleading in case of oscillations, trends, non-stationarities, outliers and data heavy tails;
- variables should be very noisy—knowing their distribution might help to design a proper version of calculations;
- causality graphs use only major connections and minor ones are not shown, even if they are important.

2.6. Signal preprocessing. Signal preprocessing in industry is essential to ensure data quality and reliability for later analysis. Raw sensor data often exhibit scale differences, noises, and transient artifacts that can hide true relationships. The Z-score normalization standardizes data, reduces the impact of outliers, and enhances algorithmic performance (Venkataanusha *et al*., 2019).

The Z-score transforms raw data into a standardized distribution with a mean of 0 and a standard deviation of 1. For a signal $X = \{x_1, x_2, \ldots, x_n\}$, the Z-score of each observation x_i is computed as

$$z_i = \frac{x_i - \mu}{\sigma}, \tag{4}$$

where μ is the mean and σ is the standard deviation of X. This normalization eliminates scale differences between variables, enabling fair comparison and reducing distortion in multivariate analyses. It addresses two key industrial challenges: noise reduction and scale harmonization.

2.7. Stationarity of time series. Stationarity is another important assumption in time series analysis, requiring that statistical properties, like mean, variance, and autocorrelation, remain constant over time (Semmlow, 2018). Non-stationary data, characterized by trends, seasonality, or structural breaks, can lead to unreliable causal inferences in methods like transfer entropy. This section introduces two statistical tests, the augmented Dickey–Fuller (ADF) and Kwiatkowski–Phillips–Schmidt–Shin (KPSS) ones, to rigorously assess stationarity in industrial datasets.

The ADF test (Dickey and Fuller, 1979) evaluates the presence of a unit root—a sign of non-stationarity. It includes lagged differences to account for autocorrelation. The regression model is

$$\Delta y_t = \alpha + \beta t + \gamma y_{t-1} + \sum_{i=1}^{p} \delta_i \Delta y_{t-1} + \epsilon_t, \tag{5}$$

where Δy_t is the differenced series, α is constant, βt represents a time trend, γ measures the unit root effect, δ_i are coefficients for lagged differences and ϵ_t is the error term.

Hypotheses:

- H_0: A unit root exists ($\gamma = 0$; non-stationary).
- H_1: There is no unit root ($\gamma < 0$; stationary).

The test statistic is compared to critical values. If the statistic is more negative than the critical value, H_0 is rejected, indicating stationarity.

The KPSS test (Kwiatkowski *et al*., 1992) supports ADF by testing for trend stationarity. It decomposes the series into a deterministic trend, a random walk, and a stationary error,

$$y_t = \xi t + r_t + \epsilon t, \tag{6}$$

where r_t is a random walk. The test statistic evaluates the variance of the random walk component.

Hypotheses:

- H_0: The series is trend-stationary.
- H_1: A unit root exists (non-stationary).

A test statistic exceeding the critical value leads to rejecting H_0, suggesting non-stationarity. Combined application of both tests provides an effective mechanism to resolve uncertainties in stationarity assessment. When both tests align, i.e., ADF rejects the null of a unit root and KPSS fails to reject the null of stationarity, they offer strong evidence for a stationary series (Charemza and Syczewska, 1998). On the other hand, if the ADF test fails to reject the unit root hypothesis and KPSS rejects its null hypothesis, the results collectively confirm non-stationarity, often driven by trends or structural breaks. When both tests are unable to reject their null hypotheses, the concerned series is usually interpreted as trend stationary. If the non-stationarity identified by KPSS is due to a deterministic trend, rather than a unit root, removing this trend by detrending usually makes the series stationary.

Conversely, when both tests reject their null hypotheses, this indicates a difference stationary process. The presence of both deterministic and stochastic components in this case can makes the test result unclear. Using first differencing usually converts the series into a stationary process.

3. Nonlinear signal decomposition

Industrial processes often generate signals characterized by nonlinearity, nonstationarity, and multiscale dynamics,

making classical linear decomposition methods, like Fourier or wavelet, ineffective. Nonlinear signal decomposition addresses linearity limitations. The decomposition of nonlinear signals is particularly crucial in scenarios where disturbances propagate through interconnected components, appearing as overlapping frequency modulations or amplitude variations. Traditional approaches fail to separate such interactions, leading to incomplete or misleading interpretations of system behavior. By contrast, adaptive decomposition methods isolate IMFs that capture localized oscillations and trends.

3.1. Median ensemble empirical mode decomposition. MEEMD addresses the inherent limitations of the original EMD method (Huang *et al.*, 1998) and its noise-assisted variant (EEMD), by introducing a robust ensemble strategy to reduce mode splitting, a phenomenon where a single oscillatory mode spreads across multiple IMFs. The EEMD enhancement by replacing the arithmetic mean with the median during the ensemble process reduces false mode divisions caused by noise-induced variability and scale overlap (Lang *et al.*, 2020).

The MEEMD algorithm starts with generation of an ensemble of noisy signal realizations, related to EEMD. For each realization, white Gaussian noise is added to the original signal, and EMD is applied to decompose the modified signal into IMFs. However, instead of averaging corresponding IMFs across the ensemble, it computes the median value at each time point for each IMF index. This median-based aggregation reduces outliers and irregular splits, as the median is resistant to extreme values in noisy realizations. The breakdown point of the median operator (50%) ensures that a mode split must occur in over half the ensemble members to remain in the final IMF. This drastically lowers the probability of artificial mode fragmentation.

MEEMD can handle non-Gaussian noise and occasional disturbances common in industrial environments. Unlike mean-based ensembling, which averages out transient artifacts unevenly, the median operator prioritizes consistency across the majority of realizations. This property is particularly beneficial in scenarios with isolated sensor faults or sudden process changes, where EEMD might incorrectly split a single disturbance into multiple IMFs.

3.2. Kernel density estimation. Probability density estimation is another key component of information-theoretic causality analysis, enabling the quantification of uncertainty and dependencies within industrial datasets. Traditional parametric approaches, which assume predefined distributional forms (e.g., Gaussian), often fail to capture complex, multimodal, or asymmetric nature of real process variables.

KDE is a nonparametric method used to estimate the probabilistic density function (PDF) of a random variable based on sampled data. Unlike histograms, which partition data into fixed bins, KDE overlays a kernel function over each data point and sums these functions to create a smooth density estimate. Bauer *et al.* (2007) employ a an Gaussian kernel, which meets core requirements: an integral equal to 1, a maximum at 0, and a decay toward infinity. For continuous data, the kernel function is defined as

$$K(x - x_i) = \frac{1}{2\pi\theta} \exp\left(-\frac{(x - x_i)^2}{2\theta^2}\right), \tag{7}$$

where θ is the kernel width. In discrete cases, data are mapped onto a grid,

$$k_i = [(n-1)\frac{x_i - x_{\min}}{x_{\max} - x_{\min}}]_{round} + 1, \tag{8}$$

which converts continuous values into discrete bins. The optimal discrete kernel width θ_{D} is computed as

$$\theta_{\mathrm{D}} = [cN^{-1/5}\sigma_x n]_{round}, \tag{9}$$

where $c = 2$, N is the sample size, and σ_x is the data's standard deviation.

The method extends to multivariate cases for joint PDF estimation. For two variables, the kernel becomes

$$K(x - x_i, y - y_i) = \frac{1}{2\pi\theta^2} \exp\left(-\frac{(x - x_i)^2 + (y - y_i)^2}{2\theta^2}\right), \tag{10}$$

enabling dependency analysis. KDE is preferred due to its higher precision, particularly with limited samples. In the context of TE, KDE enables efficient computation of conditional probabilities. A notable limitation is its computational intensity, particularly for high-dimensional data.

4. Analytical procedure

The analysis follows a multi-stage procedure shown in Fig. 1. It addresses improved alarming system coordination and root cause detection.

The method adapts to nonlinear dynamics, scales across datasets, and resists industrial noise. The workflow features four linked phases: data preparation, signal decomposition, causality analysis, and validation. Phase 1 transforms raw industrial signals into a standardized analysis format. Then, normalization removes scale differences. Phase 2 uses MEEMD to separate noise signals. IMFs reveal temporal scales and disturbance pathways. Phase 3 starts with delay estimation using both the CC and MI methods. TE quantifies directional information flow between variables.

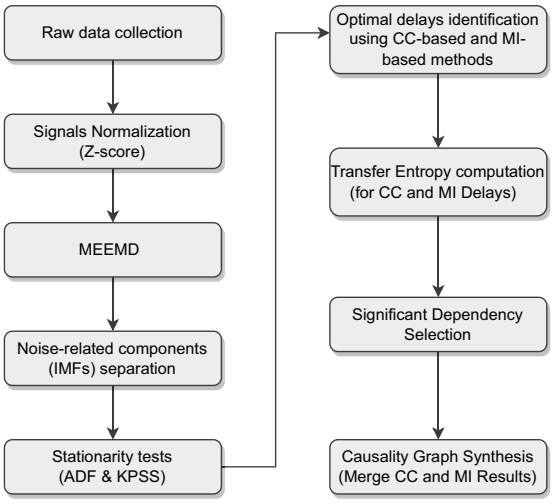

Fig. 1. Developed root cause analysis algorithm.

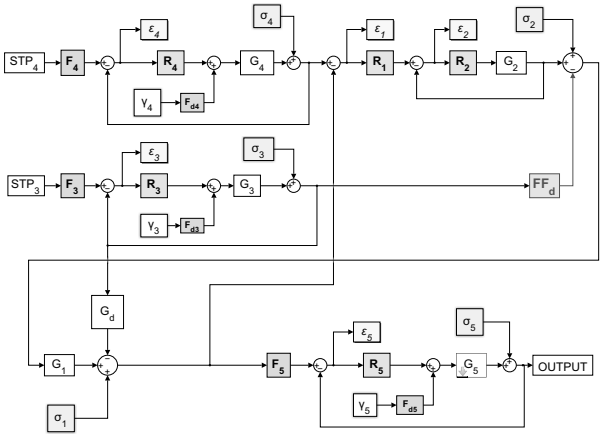

Fig. 2. Simulated multi-loop PID-based control layout.

5. Experimental validation

The proposed methodology is validated using two experiments: an artificial multi-loop control system simulated in Matlab and a Tennessee Eastman Process case study—a widely recognized benchmark in industrial process monitoring (Downs and Vogel, 1993). The simulation experiment describes all steps, while the TEP focuses on method validation.

5.1. Simulation experiment. The Simulink model (Falkowski and Domański, 2023) represents a multi-loop control system that emulates industrial process dynamics through five interconnected control loops (each controlled by PID algorithms): four PID controllers (R_1, R_2, R_3, R_4) and one PI controller (R_5), each of which is responsible for a separate process dynamics. The model utilizes linear transfer functions for process units and feedforward filters, enabling the study of interactions between loops.

The model's architecture, presented in Fig. 2, integrates control loops with distinct transfer functions which are represented as linear models:

$$
\begin{aligned}
G_1(s) &= \frac{1}{0.15s+1},\\
G_2(s) &= \frac{0.25(-s+1)}{s(2s+1)},\\
G_3(s) &= \frac{1}{(s+1)(0.04s^2+0.04s+1)},\\
G_4(s) &= \frac{1}{(s+1)^4},\\
G_5(s) &= \frac{1}{(0.2s+1)^2}e^{-s},
\end{aligned}
$$

Table 1. Controller parameters.

	R_1	R_2	R_3	R_4	R_5
P	0.2	2	0.13	0.27	0.01
I	0.01	0.2	0.5	0.61	0.2
D	0.02	–	0.08	0.21	–
N	10	–	10	100	–

$$G_d(s) = \frac{-0.25(-s+1)}{s(s+1)(2s+1)}. \tag{11}$$

The feedforward filters are expressed as

$$
\begin{aligned}
F_3(s) &= \frac{1}{4s^2+3.2s+1}, & F_4(s) &= \frac{1}{s^2+1.2s+1},\\
F_5(s) &= \frac{1}{4s^2+2s+1}, & F_{d3}(s) &= \frac{1}{2s+1},\\
F_{d4}(s) &= \frac{0.1}{s+1}, & F_{d5}(s) &= \frac{4}{2s+1}.
\end{aligned} \tag{12}
$$

The controllers are tuned using the parameters shown in Table 1.

The model generates time-series of control errors under mixed disturbance conditions to simulate real-world industrial noise and oscillatory behaviors:

- Gaussian additive noise $\mathcal{N}(0, \sigma_i)$ to represent sensor noises,
- Cauchy heavy-tailed disturbances (Nadarajah, 2011) to simulate irregular outliers and extreme deviations.

The combined effect of these disturbances results in non-stationary, nonlinear data with noticeable outliers and temporary trends, as shown in Fig. 3.

5.1.1. Simulation results. The model generates time-series for five control errors errors (ϵ_1 to ϵ_5), which are used as raw input data for the analysis. In order

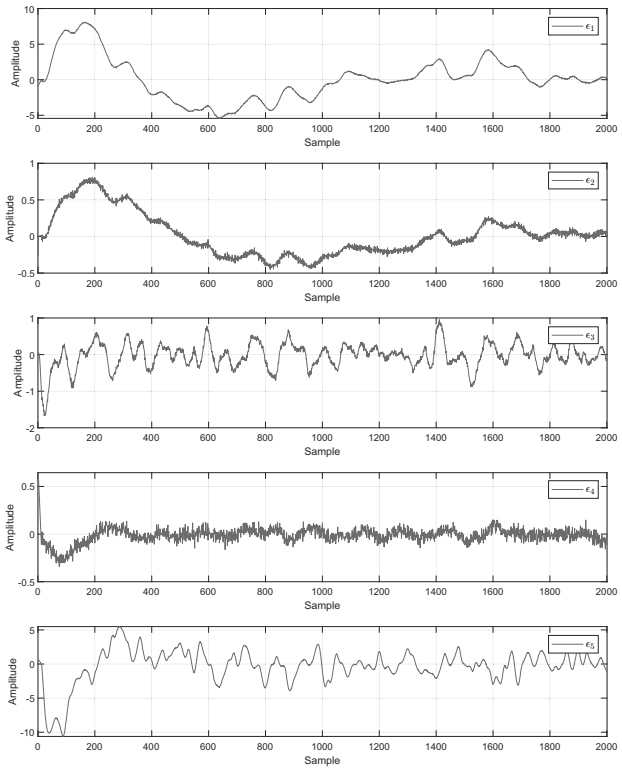

Fig. 3. Control errors time series.

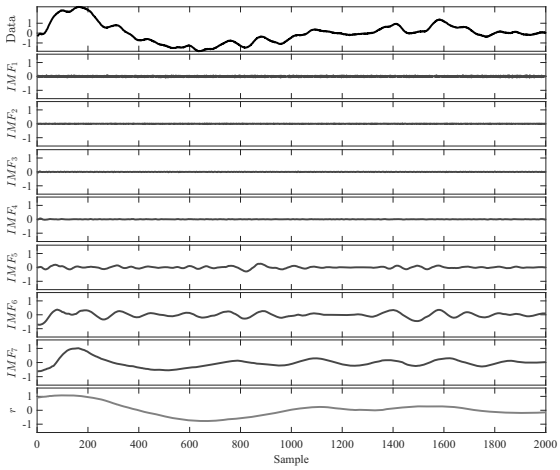

Fig. 4. Decomposition results for ϵ_1.

Table 2. ADF and KPSS tests results.

-	IMF1	IMF2	IMF3	IMF4	RAW
ϵ_1	✓	✓	✓	✓	✗
ϵ_2	✓	✓	✓	✓	✗
ϵ_3	✓	✓	✓	✓	✗
ϵ_4	✓	✓	✓	✓	✗
ϵ_5	✓	✓	✓	✓	✗

to standardize the measurement scale, normalization is performed using the Z-score method. Next, MEEMD decomposes signals into interpretable components, followed by careful IMF selection to keep features critical for causality analysis. The process ensures that high-frequency components are preserved based on their importance to root cause identification. The key parameters of the method are as follows:

- ensemble size: 200,
- amplitude of the added noise: 0.2,
- IMF count: 8 (seven IMFs + residual signal).

As illustrated in Fig. 4 for ϵ_1, MEEMD separates a regulation error into IMFs representing high-frequency noise (IMF1–IMF3), mid-frequency process interactions (IMF4–IMF5), low-frequency drifts (IMF6–IMF7), and a residual signal. A similar step is conduced for other signals.

Not all IMFs are equally relevant to causal inference. In industrial settings, high-frequency components (IMF1–IMF4 in this case) often contain noise patterns. Unlike standard denoising approaches, these components are intentionally kept for causality analysis, as they may carry early signs of fault propagation or controller-induced oscillations.

Then, stationarity tests for selected IMFs should be conducted. Theoretically, after performing MEEMD itself, the extracted series should be stationary, but, to ensure that this is true, stationarity tests are performed. Final results are presented in Table 2.

As expected, unlike the raw data, the time series for IMF1–IMF4 are stationary. The last step before identifying the optimal delays is to present and discuss the distributions in histograms. A sample histogram for control error ϵ_1 IMFs is shown in Fig. 9.

IMF1 reveals a significant deviation from Gaussianity across all five variables. Such marked deviations mean that any inflexible parametric assumption, like forcing a normal distribution, would misallocate probability mass. By contrast, KDE adapts its shape to the data itself, ensuring that these features are accurately represented rather than being smoothed over or ignored.

Both IMF2 and IMF3 approximate the bell curve reasonably well for most of the variables, displaying the characteristic single peak and symmetric decline around the center. However, even here occasional outliers and subtle shoulders reveal a less-than-perfect Gaussian fit. Relying entirely on a normal model would either underestimate the weight of those outliers or oversmooth the shoulders. IMF4 represents an intermediate position between the highly non-Gaussian IMF1 and the more

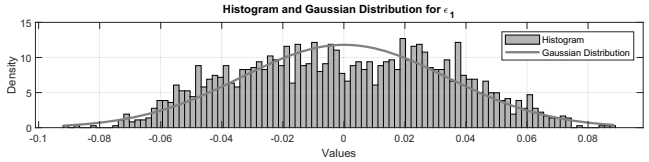

Fig. 5. IMF1

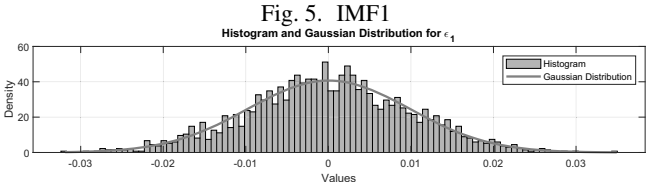

Fig. 6. IMF2

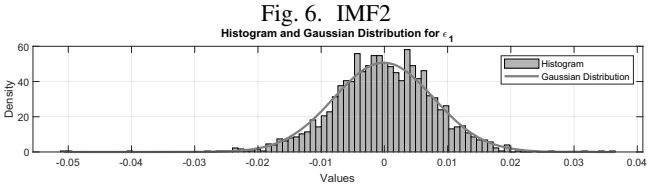

Fig. 7. IMF3

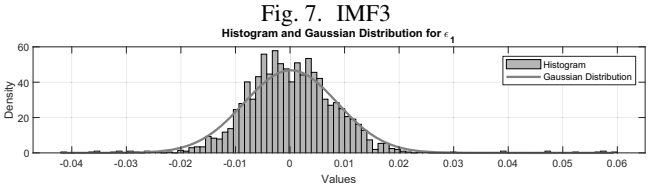

Fig. 8. IMF4

Fig. 9. Histograms and Gaussian distributions for ϵ_1 IMFs.

bell-shaped IMF2 and IMF3.

Accurate identification of temporal delays between process variables is decisive for reconstructing causal relationships, as poorly chosen time lags can lead to unclear directional dependencies. To enhance reliability, two complementary methods, CC and MI, are employed together.

Delay estimation is performed in two parallel streams: CC for linear dependencies and MI for nonlinear ones, producing separate delay matrices. Transfer entropy is then computed for each delay set, and merged to bring the final combined graph. This dual approach reduces the limitations of individual techniques, ensuring reliable delay estimation across both linear and nonlinear interactions. By cross-validating results from both methods, the methodology balances computational efficiency with sensitivity to complex industrial dynamics. Tables 3–6 summarize delays evaluation (in samples) for IMF1–IMF4, respectively.

Finally, the causality analysis forms the core of the smart alarming algorithm, transforming preprocessed data and identified delays into actionable insights about directional information flow between process variables. This stage applies transfer entropy to quantify nonlinear,

Table 3. Optimal delays for IMF1.

CC

	ϵ_1	ϵ_2	ϵ_3	ϵ_4	ϵ_5
ϵ_1	0	0	−454	0	183
ϵ_2	0	0	−779	0	−330
ϵ_3	454	779	0	−113	92
ϵ_4	0	0	113	0	−329
ϵ_5	−183	330	−92	329	0

MI

	ϵ_1	ϵ_2	ϵ_3	ϵ_4	ϵ_5
ϵ_1	0	0	−349	0	−437
ϵ_2	0	0	446	0	−460
ϵ_3	349	−446	0	339	−355
ϵ_4	0	0	−339	0	−431
ϵ_5	437	460	355	431	0

Table 4. Optimal delays for IMF2.

CC

	ϵ_1	ϵ_2	ϵ_3	ϵ_4	ϵ_5
ϵ_1	0	−1	122	0	2
ϵ_2	1	0	−454	−2	645
ϵ_3	−122	454	0	729	5
ϵ_4	0	2	−729	0	−23
ϵ_5	−2	−645	−5	23	0

MI

	ϵ_1	ϵ_2	ϵ_3	ϵ_4	ϵ_5
ϵ_1	0	−1	−455	0	399
ϵ_2	1	0	285	−2	293
ϵ_3	455	−285	0	455	467
ϵ_4	0	2	−455	0	−427
ϵ_5	−399	−293	−467	427	0

asymmetric dependencies. Based on the decomposed IMFs and calculated lags, the methodology isolates statistically significant causal pathways.

To make sure that the methodology is transparent, TE values are computed separately for each delay estimation method, which gives two individual sets of results. These computations are performed across all IMFs (IMF1–IMF4) and variable pairs (ϵ_1–ϵ_5). Results are shown in Tables 7–10. The NaN and Inf values in the TE tables for IMF3 and IMF4 come from from lower frequency signal dynamics and numerical instabilities during entropy computation. Practically, these values are treated as zero.

The proposed significant dependency selection (SDS) method aims at detection of the most likely relations by aggregating multi-scale analysis of TE among all the selected IMFs. The technique addresses the inherent issues of noise, temporary dynamics, and uncertain dependencies. It aggregates and weights the

Table 5. Optimal delays for IMF3.

CC

	ϵ_1	ϵ_2	ϵ_3	ϵ_4	ϵ_5
ϵ_1	0	−2	2	0	4
ϵ_2	2	0	−2	2	7
ϵ_3	−2	2	0	229	2
ϵ_4	0	−2	−229	0	5
ϵ_5	−4	−7	−2	−5	0

MI

	ϵ_1	ϵ_2	ϵ_3	ϵ_4	ϵ_5
ϵ_1	0	−2	2	0	4
ϵ_2	2	0	−2	2	0
ϵ_3	−2	2	0	236	0
ϵ_4	0	−2	−236	0	4
ϵ_5	−4	0	0	−4	0

Table 6. Optimal delays for IMF4.

CC

	ϵ_1	ϵ_2	ϵ_3	ϵ_4	ϵ_5
ϵ_1	0	−3	−7	−12	4
ϵ_2	3	0	−4	−8	−3
ϵ_3	7	4	0	−4	−561
ϵ_4	12	8	4	0	15
ϵ_5	−4	3	561	−15	0

MI

	ϵ_1	ϵ_2	ϵ_3	ϵ_4	ϵ_5
ϵ_1	0	−3	−5	1	−7
ϵ_2	3	0	−2	3	0
ϵ_3	5	2	0	−491	−304
ϵ_4	−1	−3	491	0	6
ϵ_5	7	0	304	−6	0

Table 7. Transfer entropy values between variables for IMF1.

CC

	ϵ_1	ϵ_2	ϵ_3	ϵ_4	ϵ_5
ϵ_1	–	0.013	0.005	0.011	0.054
ϵ_2	0.012	–	0.005	0.027	0.005
ϵ_3	0.049	0.048	–	0.004	0.053
ϵ_4	0.010	0.031	0.048	–	0.006
ϵ_5	0.005	0.053	0.006	0.048	–

MI

	ϵ_1	ϵ_2	ϵ_3	ϵ_4	ϵ_5
ϵ_1	–	0.013	0.006	0.011	0.005
ϵ_2	0.012	–	0.047	0.027	0.006
ϵ_3	0.051	0.005	–	0.048	0.005
ϵ_4	0.010	0.031	0.006	–	0.006
ϵ_5	0.052	0.051	0.051	0.048	–

Table 8. Transfer entropy values between variables for IMF2.

CC

	ϵ_1	ϵ_2	ϵ_3	ϵ_4	ϵ_5
ϵ_1	–	0.007	0.074	0.009	0.073
ϵ_2	0.173	–	0.007	0.009	0.084
ϵ_3	0.007	0.070	–	0.077	0.081
ϵ_4	0.009	Inf	0.010	–	0.007
ϵ_5	0.009	0.009	0.008	0.082	–

MI

	ϵ_1	ϵ_2	ϵ_3	ϵ_4	ϵ_5
ϵ_1	–	0.007	0.009	0.009	0.093
ϵ_2	0.173	–	0.072	0.009	0.087
ϵ_3	0.075	0.007	–	0.077	0.091
ϵ_4	0.009	Inf	0.008	–	0.009
ϵ_5	0.009	0.009	0.008	0.084	–

Table 9. Transfer entropy values between variables for IMF3.

CC

	ϵ_1	ϵ_2	ϵ_3	ϵ_4	ϵ_5
ϵ_1	–	NaN	NaN	NaN	0.112
ϵ_2	NaN	–	NaN	NaN	NaN
ϵ_3	NaN	NaN	–	0.098	NaN
ϵ_4	NaN	NaN	0.010	–	0.125
ϵ_5	Inf	NaN	NaN	Inf	–

MI

	ϵ_1	ϵ_2	ϵ_3	ϵ_4	ϵ_5
ϵ_1	–	Nan	Nan	Nan	0.112
ϵ_2	Nan	–	Nan	Nan	Nan
ϵ_3	Nan	Nan	–	0.087	Nan
ϵ_4	Nan	Nan	0.009	–	0.116
ϵ_5	Inf	Nan	Nan	Inf	–

Table 10. Transfer entropy values between variables for IMF4.

CC

	ϵ_1	ϵ_2	ϵ_3	ϵ_4	ϵ_5
ϵ_1	–	NaN	Inf	NaN	NaN
ϵ_2	NaN	–	NaN	NaN	NaN
ϵ_3	-Inf	NaN	–	NaN	0.017
ϵ_4	NaN	NaN	NaN	–	NaN
ϵ_5	NaN	NaN	0.204	NaN	–

MI

	ϵ_1	ϵ_2	ϵ_3	ϵ_4	ϵ_5
ϵ_1	–	Nan	Inf	Nan	Nan
ϵ_2	Nan	–	Nan	Nan	Nan
ϵ_3	Nan	Nan	–	0.012	0.016
ϵ_4	Nan	Nan	0.182	–	Nan
ϵ_5	Nan	Nan	0.233	Nan	–

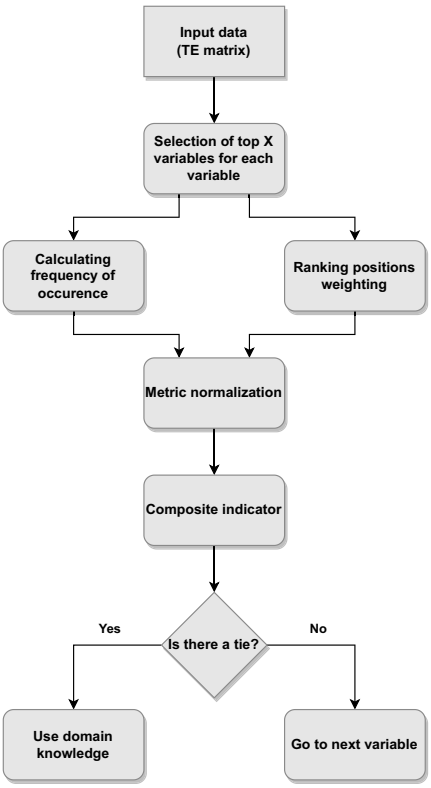

Fig. 10. SDS algorithm.

dependencies found among various IMFs obtained from MEEMD.

SDS works in three phases. It starts with the extraction of the top dependencies for each IMF by TE value ranking with the exclusion of self-loops. For each IMF, the X highest ranked variables with the greatest TE values are taken and weighted according to their rank position, i.e., five points for the highest ranked dependency and then linearly decreasing. This is motivated by the assumption that dependencies that frequently appear highest across IMFs represent more likely real causal interactions. The graphical representation of the algorithm is shown in Fig. 10.

Next, SDS combines the results of all IMFs with two normalized metrics: the frequency of occurrence and cumulative weighted TE scores. Frequency is the rate of occurrence of the dependency among the top candidate sets across, while cumulative scores jointly integrate the TE scores with the positional weights. Each one is normalized to the $[0, 1]$ range before they are combined into a single composite measurement. Finally, the method is cross-checked by an expert to address uncertainties due to the existence of ties in composite scores. The output of the algorithm is a ranked list. The algorithm overcomes the weaknesses of single-scale methods and increases the reliability of industrial dependency detection.

Causality graphs are constructed in order to represent

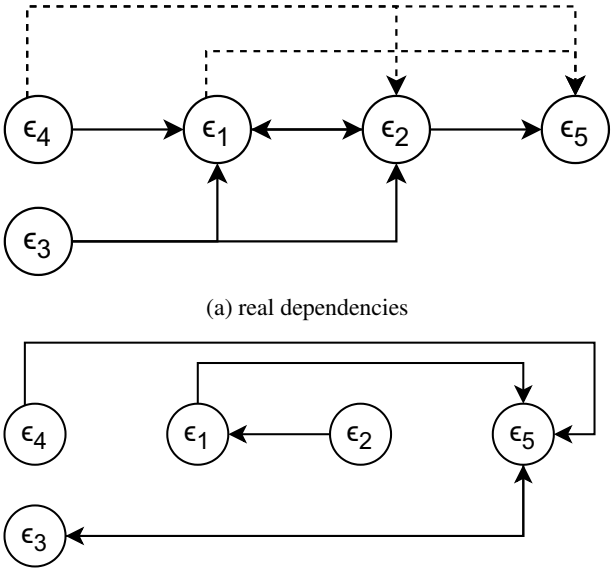

(a) real dependencies

(b) obtained TE-based graph

Fig. 11. Causality graphs for the simulated system.

and validate the directed dependencies that the analysis identifies. The causality graphs sketched in Fig. 11 compare real direct (e.g., $\epsilon_4 \rightarrow \epsilon_1$) and indirect (e.g., $\epsilon_1 \rightarrow \epsilon_5$) relationships between control errors with obtained graph.

The validation of the smart alarming algorithm on the Simulink model evaluates the alignment between the theoretical causality graph and the empirical causality one. It focuses on the system's predefined direct and indirect interactions. While the theoretical graph includes both direct (solid edges) and indirect (dashed edges) pathways, the empirical one prioritizes direct causal links by selecting the strongest dependency for each variable, omitting weaker or indirect connections. The analysis of the results shows the following:

- Matched direct connections:
  - $\epsilon_2 \rightarrow \epsilon_1$ is correctly identified;
  - partial matches:
    - The empirical graph infers $\epsilon_4 \rightarrow \epsilon_5$ and $\epsilon_1 \rightarrow \epsilon_5$, which are indirect in the theoretical graph. These are treated as direct dependencies due to the algorithm's focus on immediate information flow.
- Unmatched connections:
  - theoretical direct links like $\epsilon_3 \rightarrow \epsilon_1$ and $\epsilon_1 \rightarrow \epsilon_2$ are absent in the empirical graph, as the "strongest connection per variable" convention discards weaker/multiple edges;

– bidirectional links (e.g., $\epsilon_3 \leftrightarrow \epsilon_5$) in the empirical graph are not present in the theoretical model.

The alignment between the empirical and theoretical graphs can be interpreted through three points of view, leading to different consistency percentages:

1. lenient interpretation (including indirect as valid):
   - theoretical total connections: 9 (six direct + three indirect),
   - empirical connections matching theoretical (direct or indirect): 3,
   - match: $\frac{3}{9} \approx 33\%$;
2. alternative interpretation (empirical accuracy):
   - empirical connections: 5,
   - correct empirical connections: 3,
   - match: $\frac{3}{5} \approx 60\%$.

The path consistency between the empirical and real causality graphs ranges from 33% to 60%, depending on whether indirect pathways are interpreted as valid matches for direct empirical links. The lower bound reflects alignment considering all theoretical connections, while the upper one measures the proportion of empirical links to theoretical pathway.

5.2. Tennessee Eastman Process case study. The TEP is a well-known benchmark model for industrial process control studies, designed to simulate the complexities of a real chemical plant (Downs and Vogel, 1993). It provides a realistic framework for evaluating control strategies, fault detection methods, and optimization algorithms under dynamic and nonlinear conditions. Its structure, shown in Fig. 12, simulates a reactor/separator/recycle system with multiple interacting units. The process comprises five interconnected units: a reactor, a condenser, a vapor-liquid separator, a compressor, and a stripper.

Its key features include the following:

- 12 manipulated variables (MVs) and 41 process variables (PVs);
- six production modes with varying G/H mass ratios (50/50, 10/90, 90/10) and production rates;
- reaction kinetics following Arrhenius temperature dependence, and vapor-liquid equilibria adhering to Raoult's law;
- equipment limits (e.g., reactor pressure $\leq$ 2895 kPa) and product quality requirements (e.g., composition variability $\leq \pm 5$ mol%);

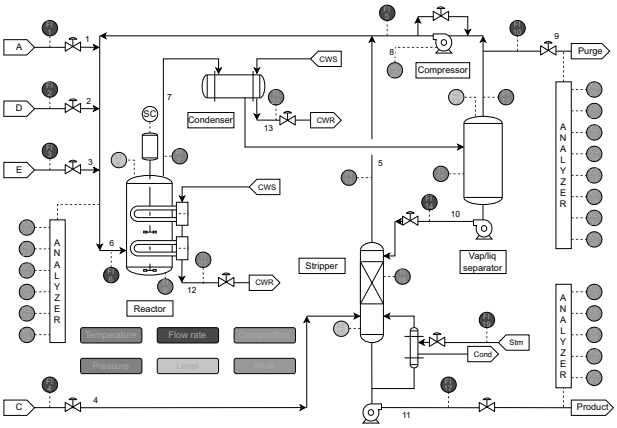

Fig. 12. Tennessee Eastman Process diagram.

- 20 predefined disturbance scenarios (IDV1–IDV20), categorized to step changes, random variations, and equipment malfunctions, which simulate realistic industrial failures.

5.2.1. Case study results. The TEP evaluates smart alarming performance in real-world. The IDV(6) scenario is selected for validation due to its operational importance, clearly identifiable root cause, and cascading downstream impact. It simulates a sudden loss of the A feedstock supply, which is a common fault in chemical plants. It triggers rapid pressure drops in the reactor, level fluctuations in the separator, and composition deviations in the purge stream, and offers a clear causal pathway (feed loss $\rightarrow$ reactor instability $\rightarrow$ separator/purge alarms). The workflow is organized as follows:

1. *Causality graph construction*. Generate a reference TE-based causality graph for normal operation data to capture inherent variable relationships.
2. *Failure scenario execution*. Simulate the chosen disturbance and extract time-series data for all relevant process variables.
3. *Causal pathway identification*. Starting from the known root cause variable, trace the predefined causal propagation path through the baseline graph.
4. *Trajectory analysis*. Plot measurement trajectories for variables along the causal path, including the root variable and downstream variables.
5. *Alarm sequence validation*. Verify that alarms are triggered in the order that matches the order of propagation in the causal graph.

While the proposed algorithm advances causality-driven diagnostics, several methodological limitations are noted:

- *Computational complexity*. Optimal delay values identification and TE calculations, particularly with KDE and multiple IMFs, demand significant computational resources. High-dimensional systems (41 variables) increase the challenges associated with the runtime environment, limiting real-time use.
- *Signal decomposition sensitivity*. MEEMD performance depends on the choice of parameters (ensemble size, noise amplitude). Wrong choices may induce mode mixing or weaken critical noise-related components, misleading causal links.
- *Stationarity assumptions*. TE assumes stationarity, which requires preprocessing. Conversely, such transformations may affect detection correctness.
- *Delay estimation trade-offs*. CC and MI balance linear and nonlinear delay detection, but remain sensitive to misalignment in highly non-Gaussian cases.

These limitations underscore the current suitability of the algorithm for offline or semi-real-time diagnostics rather than high-frequency monitoring. Nevertheless, the methodology provides a solid foundation for causality-aware alarm management in industrial settings.

Following data preprocessing, decomposition, and delay estimation, raw causality diagrams are obtained. Figures 13 and 14 present causality graphs overlaid on the TEP for both delay estimation methods. The dashed lines indicate links that are at a similar level of dependency.

Figure 15 shows merged causality graph mapping disturbance propagation pathways across the TEP. Arrows are color-coded to distinguish consensus connections (thick grey dotted line: validated by both the mutual information and cross-correlation delay estimation methods) from MI-exclusive links (thin grey dashed line: detected only by MI). Dual-method validation ensures high confidence in green connections, which represent robust dependencies.

Knowing that the source of the disturbance is the loss of feed A flow, the path identification should start with the analysis of the propagation of the flow of feed A measurement, marked with the number 1. The algorithm isolates XMEAS(1) (Feed A Flow in Stream 1) as the node, with a dotted grey arrow pointing to XMEAS(13) (Separator Pressure). A subsequent dotted grey arrow connects XMEAS(13) to XMEAS(29) (Purge Gas Composition A), forming the primary causal pathway,

$$\text{XMEAS(1)} \xrightarrow{green} \text{XMEAS(13)} \xrightarrow{green} \text{XMEAS(29)}.$$

Figure 16 shows the propagation along causal pathway:

1. sample 0: XMEAS(1) exceeds its lower threshold (feed loss detected);

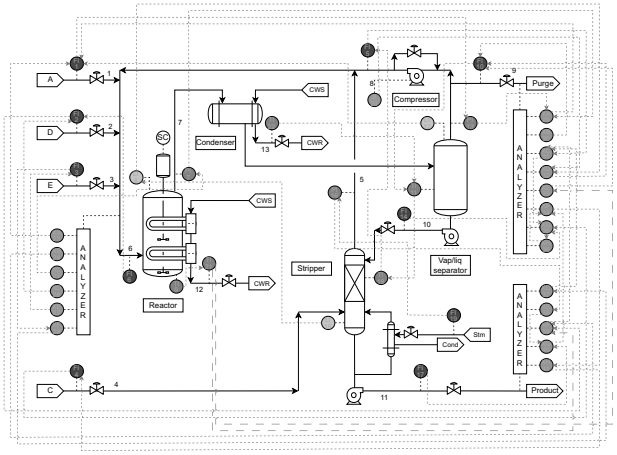

Fig. 13. Causality graphs for the TEP: CC-based delays.

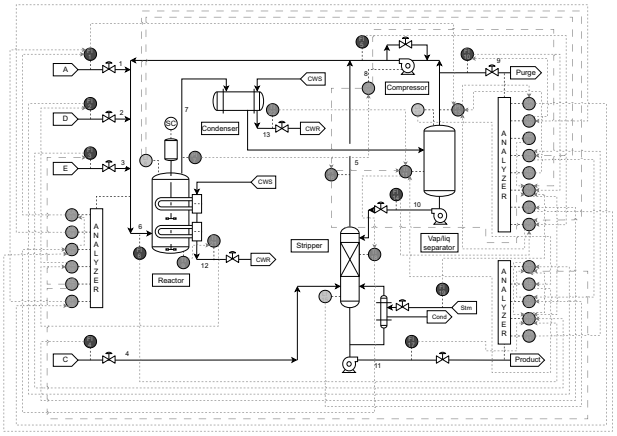

Fig. 14. Causality graphs for the TEP: MI-based delays.

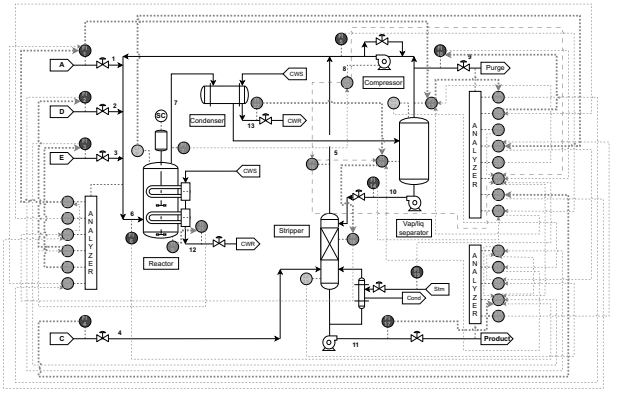

Fig. 15. Causality graph overlaid on the TEP schematic.

2. sample 29: XMEAS(13) rises above the threshold;
3. sample 57: XMEAS(29) drops below the composition alarm threshold.

This sequence aligns with the inferred causal graph,

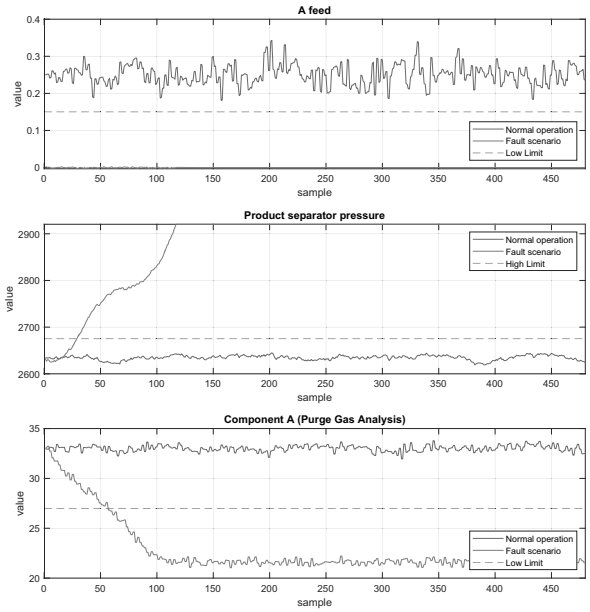

Fig. 16. Time-series XMEAS(1), XMEAS(13), and XMEAS(29) with alarm thresholds.

validating the algorithm's ability to trace disturbance propagation. The algorithm successfully reconstructs the cascading effects of the IDV(6) scenario. The results validate the methodology's potential to transform alarm management systems, prioritizing causality-driven diagnostics over traditional threshold-based.

6. Conclusions and further research

This work presented an original smart alarming algorithm designed to address the critical challenge of root cause identification in industrial systems. By integrating MEEMD and TE with dual-method delay estimation, the algorithm isolates primary disturbance sources. Its success in reconstructing causal pathways was validated on Simulink and with the application of the Tennessee Eastman Process. It demonstrates a shift from reactive threshold-based alarming to proactive, causality-driven diagnostics.

The algorithm's key strength is its ability to prioritize interpretability without sacrificing analytical rigor. By preserving noise-characterized signal components and synthesizing shared causal graphs, it provides operators with actionable insights during cascading failures.

The presented case studies and applications incorporate the transfer entropy concept into the frameworks of process assessment, diagnostics, fault detection and smart alarming. However, it should be noted that these are not the only possible applications in control engineering. Proper design of process simulators or planning of training sessions for operators are natural successors. Transfer entropy may support the design process for plantwide control systems, especially once multivariate or advanced process control strategies are targeted.

While computational complexity and threshold sensitivity remain challenges, these limitations are counterbalanced by the algorithm's modular design, which allows for future enhancements such as machine learning integration or hybrid physics-informed modeling. Its validation in simulated and near-industrial environments lays a foundation for deployment in real-world settings, where rapid root cause isolation can reduce downtime and operational risks, enhancing safety.

The proposed algorithm lays a robust basis for causality-driven alarm management, yet several paths for improvement remain. Addressing these directions could bridge the gap between academic innovation and operational practicality. Machine learning could augment the adaptability. Clustering algorithms might automate the selection of IMF thresholds. Reinforcement learning could optimize delay estimation parameters in real time, adapting to transient dynamics. Deep learning models pre-trained on historical fault data could prioritize causal pathways based on contextual patterns, reducing reliance on thresholds.

Parallelizing MEEMD and TE calculations across GPUs or distributed computing frameworks could drastically reduce runtime. Sparse KDE techniques might replace exhausting grid-based density estimation, cutting computation time while preserving accuracy. Combining data-driven causality analysis with physics-based models could resolve uncertainties such as bidirectional irregularities. Such a hybrid approach would filter misleading links and enhance interpretability, particularly in systems with closed-loop control. Lightweight MEEMD variants and optimized TE calculations could reduce memory usage, making the algorithm practical for resource-constrained hardware. Coupling with digital twin would enable predictive alarming, where causality anticipates disturbances before thresholds are exceeded.

By pursuing these directions, the algorithm could evolve into a flexible tool for Industry 4.0, turning raw data into useful information while dealing with the challenges of modern industry.

References

ANSI/ISA (2016). *ANSI/ISA-18.2-2016 (R2021): Management of Alarm Systems for the Process Industries*, American National Standard, International Society of Automation, Research Triangle Park, https://www.isa.org/products/ansi-isa-18-2-2016-management-of-alarm-systems-for.

Battiti, R. (1994). Using mutual information for selecting features in supervised neural net learning, *IEEE Transactions on Neural Networks* **5**(4): 537–550.

Bauer, M., Cox, J.W., Caveness, M.H., Downs, J.J. and Thornhill, N.F. (2007). Finding the direction of disturbance propagation in a chemical process using transfer entropy, *IEEE Transactions on Control Systems Technology* **15**(1): 12–21.

Bauer, M. and Thornhill, N. (2008). A practical method for identifying the propagation path of plant-wide disturbances, *Journal of Process Control* **18**(7): 707–719.

Beardah, C.C. and Baxter, M.J. (1996). Matlab routines for kernel density estimation and the graphical representation of archaeological data, *in* H. Kammermans and K. Fennema (Eds), *Interfacing the Past: Computer Applications and Quantitative Methods in Archaeology CAA95*, Leiden University Press, Leiden, pp. 179–184.

Chakraborty, N. and van Leeuwen, P.J. (2022). Using mutual information to measure time lags from nonlinear processes in astronomy, *Physical Review Research* **4**: 013036.

Charemza, W. and Syczewska, E. (1998). Joint application of the Dickey–Fuller and KPSS tests, *Economics Letters* **61**(1): 17–21.

Chu, K.S.K., Chew, K.W. and Chang, Y.C. (2023). Fault-diagnosis and fault-recovery system of hall sensors in brushless DC motor based on neural networks, *Sensors* **23**(9): 4330.

Dickey, D. and Fuller, W.A. (1979). Distribution of the estimators for autoregressive time series with a unit root, *Journal of the American Statistical Association* **74**(366): 427–431.

Domański, P.D. (2020). *Control Performance Assessment: Theoretical Analyses and Industrial Practice*, Springer International Publishing, Cham.

Domański, P.D. (2025). *Back to Statistics: Tail-Aware Control Performance Assessment*, CRC Press, Boca Raton.

Downs, J. and Vogel, E. (1993). A plant-wide industrial process control problem, *Computers & Chemical Engineering* **17**(3): 245–255.

Falkowski, M.J. (2022). Causality analysis incorporating outliers information, *in* P.D. Domański *et al.* (Eds), *Outliers in Control Engineering: Fractional Calculus Perspective*, De Gruyter, Berlin/Boston, pp. 133–148.

Falkowski, M.J., Domański, P.D. and Pawłuszewicz, E. (2022). Causality in control systems based on data-driven oscillation identification, *Applied Sciences* **12**(8): 3784.

Falkowski, M.J. and Domański, P.D. (2023). Causality analysis with different probabilistic distributions using transfer entropy, *Applied Sciences* **13**(10): 5849.

Ge, X. and Lin, A. (2023). Quantifying the direct and indirect interactions for EEG signals by using detrended permutation mutual information, *Chaos, Solitons & Fractals* **176**: 114155.

Hamdi, H., Rodrigues, M., Rabaoui, B. and Benhadj Braiek, N. (2021). A fault estimation and fault-tolerant control based sliding mode observer for LPV descriptor systems with time delay, *International Journal of Applied Mathematics & Computer Science* **31**(2): 247–258, DOI: 10.34768/amcs-2021-0017.

HSE (1997). The explosion and fires at the Texaco Refinery, Milford Haven, 24 July 1994: A report of the investigation by the Health and Safety Executive into the explosion and fires on the pembroke cracking company plant at the Texaco Refinery, Milford Haven on 24 July 1994, *Technical report*, Health and Safety Executive, Norwich, https://www.jesip.org.uk/wp-content/uploads/2022/03/Texaco-Refinery-Explosion.pdf.

Huang, N.E., Shen, Z., Long, S.R., Wu, M.C., Shih, H.H., Zheng, Q., Yen, N.C., Tung, C. and Liu, H.H. (1998). The empirical mode decomposition and the Hilbert spectrum for nonlinear and non-stationary time series analysis, *Proceedings of the Royal Society of London A: Mathematical, Physical and Engineering Sciences* **454**(1971): 903–995.

Jadidi, Z., Hagemann, J. and Quevedo, D. (2022). Multi-step attack detection in industrial control systems using causal analysis, *Computers in Industry* **142**: 103741.

Jungwirth, P. and Hahs, D.W. (2019). Transfer entropy quantifies information leakage, *2019 SoutheastCon, Huntsville, USA*, pp. 1–6.

Knockaert, L. and Dhaene, T. (2008). Causality determination and time delay extraction by means of the eigenfunctions of the Hilbert transform, *12th IEEE Workshop on Signal Propagation on Interconnects, Avignon, France*, pp. 1–4.

Kóscielny, J.M. and Bartyś, M. (2025). Investigating the problem of misdiagnosis in model-based fault diagnosis, *International Journal of Applied Mathematics & Computer Science* **35**(2): 235–250, DOI: 10.61822/amcs-2025-0017.

Kościelny, J., Bartyś, M., Syfert, M., and Sztyber, A. (2022). Graph theory-based approach to the description of the process and the diagnostic system, *International Journal of Applied Mathematics & Computer Science* **32**(2): 213–227, DOI: 10.34768/amcs-2022-0016.

Kwiatkowski, D., Phillips, P., Schmidt, P. and Shin, Y. (1992). Testing the null hypothesis of stationarity against the alternative of a unit root, *Journal of Econometrics* **54**(1–3): 159–178.

Kwon, O. and Yang, J.-S. (2008). Information flow between stock indices, *Europhysics Letters* **82**(6): 68003.

Labib, A. (2014). BP Texas City disaster, *in* A. Labib (Ed.), *Learning from Failures*, Butterworth-Heinemann, Oxford, pp. 83–95.

Lang, X., ur Rehman, N., Zhang, Y., Xie, L. and Su, H. (2020). Median ensemble empirical mode decomposition, *Signal Processing* **176**: 107686.

Li, W., Lin, Q., Zhang, C.Y., Han, Y., Li, H. and Calhoun, V. D. (2024). Estimation of complete mutual information exploiting nonlinear magnitude-phase dependence: Application to spatial FNC for complex-valued FMRI data, *Journal of Neuroscience Methods* **409**: 110207.

Lindner, B., Auret, L. and Bauer, M. (2017a). Investigating the impact of perturbations in chemical processes on data-based causality analysis. Part 1: Defining desired performance of causality analysis techniques, *IFAC-PapersOnLine* **50**(1): 3269–3274.

Lindner, B., Auret, L. and Bauer, M. (2017b). Investigating the impact of perturbations in chemical processes on data-based causality analysis. Part 2: Testing Granger causality and transfer entropy, *IFAC-PapersOnLine* **50**(1): 3275–3280.

Maican, C.A., Pană, C.F., Pătrașcu-Pană, D.M. and Rădulescu, V.M. (2025). Review of fault detection and diagnosis methods in power plants: Algorithms, architectures, and trends, *Applied Sciences* **15**(11): 6334.

Nadarajah, S. (2011). Making the Cauchy work, *Brazilian Journal of Probability and Statistics* **25**(1): 299–120.

Parvez, M.R., Roohi, M.H., Guo, Z. and Xu, F. (2025). Proactive management of industrial alarm floods: A reinforcement learning framework for early prediction and operator support, *Control Engineering Practice* **161**: 106341.

Rahmanian, M. and Mansoori, E. (2022). An unsupervised gene selection method based on multivariate normalized mutual information of genes, *Chemometrics and Intelligent Laboratory Systems* **222**: 104512.

Rodrigo, V., Chioua, M., Hägglund, T. and Hollender, M. (2016). Causal analysis for alarm flood reduction, *IFAC-PapersOnLine* **49**(7): 723–728.

Ruiz, D., Nougués, J.M. and Puigjaner, L. (2001). Fault diagnosis support system for complex chemical plants, *Computers & Chemical Engineering* **25**(1): 151–160.

Schreiber, T. (2000). Measuring information transfer, *Physical Review Letters* **85**(2): 461–464.

Semmlow, J. (2018). Stochastic, nonstationary, and nonlinear systems and signals, *in* J. Semmlow (Ed.), *Circuits, Signals and Systems for Bioengineers*, 3rd Edn, Academic Press, Burlington, pp. 449–489.

Seyed Alinezhad, H., Roohi, M.H. and Chen, T. (2022). A review of alarm root cause analysis in process industries: Common methods, recent research status and challenges, *Chemical Engineering Research and Design* **188**: 846–860.

Shannon, C.E. (1948). A mathematical theory of communication, *The Bell System Technical Journal* **27**(4): 623–656.

Shojaie, A. and Fox, E.B. (2022). Granger causality: A review and recent advances, *Annual Review of Statistics and Its Application* **9**: 289–319.

Skillman, G.R. and Rempe, J.L. (2021). The Three Mile Island Unit 2 accident, *in* E. Greenspan (Ed.), *Encyclopedia of Nuclear Energy*, Elsevier, Oxford, pp. 17–29.

Tongal, H. and Sivakumar, B. (2021). Forecasting rainfall using transfer entropy coupled directed–weighted complex networks, *Atmospheric Research* **255**: 105531.

Venkataanusha, P., Anuradha, C., Murty, D. and Chebrolu, S. (2019). Detecting outliers in high dimensional data sets using z-score methodology, *International Journal of Innovative Technology and Exploring Engineering* **9**(1): 48–53.

Vicente, R., Wibral, M., Lindner, M. and Pipa, G. (2011). Transfer entropy—A model-free measure of effective connectivity for the neurosciences, *Journal of Computational Neuroscience* **30**(1): 45–67.

Vogel-Heuser, B., Schütz, D. and Folmer, J. (2015). Criteria-based alarm flood pattern recognition using historical data from automated production systems (APS), *Mechatronics* **31**: 89–100.

Yang, F., Duan, P., Shah, S. and Chen, T. (2014). *Capturing Connectivity and Causality in Complex Industrial Processes*, Springer International Publishing AG, Cham.

Zhang, X., Hu, W. and Yang, F. (2022). Detection of cause–effect relations based on information granulation and transfer entropy, *Entropy* **24**(2): 212.

Zhong, Y. and Li, X. (2025). Network information security protection method based on additive Gaussian noise and mutual information neural network in cloud computing background, *Egyptian Informatics Journal* **30**: 100673.

Hubert Pisiecki was born in 2000 in Białystok, Poland. He received his BEng and MSc degrees in automatic control and robotics from Warsaw University of Technology, Poland, in 2023 and 2025, respectively. His research interests include control systems, industrial diagnostics, causality analysis, and data-driven approaches in industrial automation.

Paweł D. Domański was born in 1967 in Warsaw, Poland. He received his MSc degree in 1991, his PhD degree in 1996 and his DSc degree in 2018, all in control engineering, from the Warsaw University of Technology. Since 1991 he has been working at the Institute of Control and Computational Engineering, Warsaw University of Technology. Besides engaging in scientific research, he has participated in dozens of industrial implementations of advanced process control (APC) and optimization in power and chemical industries. He is the (co-)author of four books and more than 150 publications. His main research interest is in industrial APC applications, control performance quality assessment and optimization. Currently, his focus is shifting toward multi-agent modeling for supply chain management processes.

Received: 17 October 2025
Revised: 11 February 2026
Accepted: 27 February 2026